Electrostatic Actuators With Expanded Tuning Range Due to Biaxial Intrinsic Stress Gradients

Gary D. Gray, Matthew J. Morgan, and Paul A. Kohl, *Member, IEEE*

***Abstract*—A stress gradient was induced in two directions (through the plane of the beam and along its length) to produce a beam deflection of varying curvature. The stress gradient in the through-plane direction was produced by altering the conditions during electroplating and in the in-plane direction through lithographic patterning. The pull-down characteristics of four electrostatic actuator designs were analyzed. The in-plane stress gradient, along the length of the beam, significantly improved the tuning range compared with devices containing spatially uniform stress. This advance has greatly eased the instability problem of electrostatically actuated beams. The tuning range of a device with two hinges and a square front improved from less that 33% to 70%. Devices with two hinges and elliptical front improved to 45% tuning range and those with rectangular shape improved to 65% stability. This advance has been applied to actuators for RF tuners. Voltage cycling impacted only the initial cycling of the actuator. [921]**

I. Introduction

MICROELECTROMECHANICAL system (MEMS) technology enables the batch fabrication of miniature mechanical structures, devices, and systems. Most MEMS designs use electrostatic, electromagnetic, thermal-electric, or magnetostatic actuation to move the micromachined parts [1]. Electrostatically activated cantilever beams have been used as variable capacitors [2], [3].

A simple schematic of such a device is shown in Fig. 1. In this device, a movable top electrode acts as one plate of the capacitor, and the fixed-position bottom electrode acts as the other plate. The top electrode is a bimetallic structure that has some positive vertical (y-direction) initial deflection due to internal stresses present in the beam during fabrication. When the top layer of the bimetallic is at a higher stress state (in tension), release of the structure results in a constriction of the stressed layer and vertical bending of the device in the upward direction. Application of a potential difference between the bottom electrode and the movable beam (top electrode), resulting in a charge distribution between the two electrodes. The balance between an attractive, electrostatic force and a mechanical, restoring force controls the position of the top electrode. A problem occurs when the nonlinear electrostatic force overcomes the mechanically elastic, upward force and causes the beam to become unstable and snap-down [2], [3].

This snap-down instability problem generally occurs early in the movement of such a device from its initial position and therefore severely limits the tunable range of the actuator. A one-dimensional spring model can illustrate this action [3].

Consider the case of two electrodes aligned parallel to each another and separated by a gap distance, d. One electrode is fixed, and a linear elastic restoring force suspends the other electrode. The electrostatic attractive force is nonlinear with y, since it depends on $1/(d-y)^2$, while the mechanical restoring force is linear with y. Instability results in this system. The system becomes unstable when the potential bias applied to the bottom electrode equals the pull-in voltage $V_{\text{pull-in}}$ given in (1). At the critical point of instability, the distance between the plates is $(2/3)(d)$.

$$V_{\text{pull-in}} = \left[\frac{8kd^3}{27\varepsilon A}\right]^{1/2} \tag{1}$$

where epsilon is the permittivity of the material between the electrodes, A is the area of the electrodes, k is the spring constant of the elastic restoring force, and d is the initial gap distance.

A large tunable range between the electrodes translates into a larger capacitance tuning range when the device is used as a variable capacitor and is highly desired. Methods have been introduced to extend the tuning range of electrostatic actuators. Hung and Senturia present two techniques of extending the tuning range [4]. In a method called leveraged bending, an electrostatic force was applied to a portion of the beam, and the rest of the beam was used as a lever to position specific parts of the beam through a large range of motion [4]. A small electrode was placed near the anchors and did not cover the entire area of the beam. While the portion of the beam that experienced the electrostatic force moved less than 1/3 (point of instability) of the initial gap distance downward, the tip of the beam moved the full distance. The leveraged bending technique is very sensitive to the residual tensile stress in the beam [4]. When a beam has a high tensile stress, the portion of the beam that acts as a lever remains flat and decreases the motion of the entire beam. In the strain stiffening method [4], the tensile stress in the beam increases upon application of an applied voltage because of increasing strain. This makes the beam become stiffer with deflection and enhances the tuning range.

Recently, Chinthakindi demonstrated fabrication of cantilevers made out of a single metal with a stress gradient in the through-plane direction. By varying the grain size of the gold, different states of stress were used in a stack to generate

Manuscript received August 9, 2002; revised May 27, 2003. This material is based upon work supported by the Defense Advanced Research Projects Agency, Defense Science Office, DARPA Order J607 Total Agile RF Sensor Systems (TASS) issued by DARPA/CMD under Contract #MDA972-00-C-0010. Subject Editor G. K. Fedder.

The authors are with the School of Chemical Engineering, Georgia Institute of Technology, Atlanta, GA 30332-0100 USA (e-mail: paul.kohl@che.gatech.edu).

Digital Object Identifier 10.1109/JMEMS.2003.823231

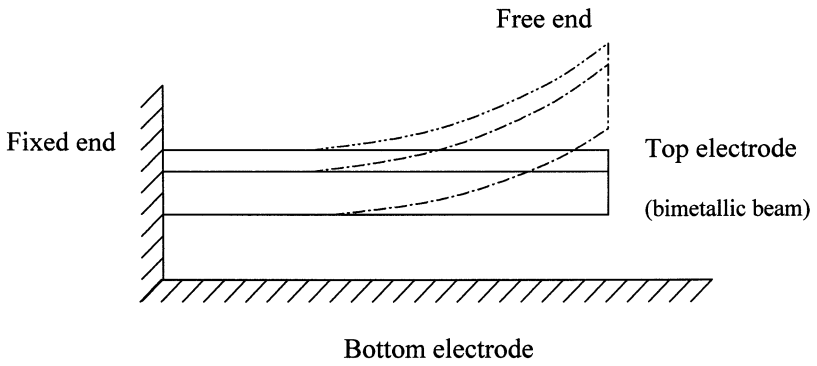

Fig. 1. Diagram of a bimetallic gold beam under influence of electrostatic field.

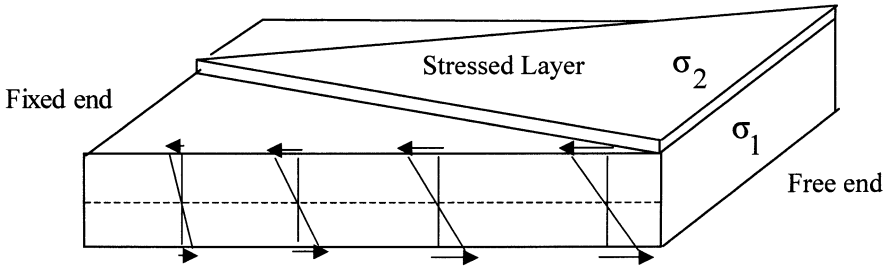

Fig. 2. Diagram of a bimetallic gold beam with patterned stressed hard gold.

out of plane curvature [3]. However, the limited tuning range [see (1)] resulted in little stable movement. In this paper, a significant increase in tuning range is demonstrated by forming a stress gradient in two directions: along the length of the beam (in-plane), along with the more traditional through-plane gradient. In previous work [2], [3], highly stressed hard gold was deposited on the low-stress soft gold layer. However, the stress profile is independent of position along the beam length. In this study, the stress gradient using the hard gold approach was formed in such a manner so as to induce an additional stress component along the length of the beam (x-direction) by depositing a spatially varying gold layer. The stressed hard gold was applied in the shape of an isosceles triangle on the beam, as shown in Fig. 2. The vertex of the triangle begins at the hinges and extends out to the end of the beam. In this way, a larger y-axis stress gradient exists at the tip of the beam than at the hinge. In particular, the slope of the stress profile at the tip is identical to that of the uniformly stressed beam, but vanishes at the hinge, resulting in a curvature of the beam that increases along the beam length. This triangular hard-gold pattern is one example, a demonstration, of the two-axis stress gradient approach. Many other patterns could be used, depending on the particular application. This patterned hard gold shape changes the pull-down characteristics of the beam. The effect of temperature on the operation of these devices was also investigated. Since the devices are made from all gold, little effect of temperature is anticipated. In this work, a general approach to improved electrostatic beam performance is demonstrated. One target application is RF MEMS actuators. It should also be noted that the low-stress, soft gold and the high-stress, hard gold are widely used in the electronics industry. The mechanical properties are controlled by grain size of the gold. The grain size is highly stable with time and has been in wide-scale use for decades [5]. RF MEMS devices may be used in place of traditional solid-state components that require high power consumption and a high manufacturing cost. This is especially evident in military applications where, in some cases, a single MEMS component replaces and outperforms an entire solid-state circuit [1]. RF MEMS devices offer lower power consumption and increased functionality in military applications where a high degree of frequency agility and sharp filtering is critical.

II. Theory

To determine the expected shape of a cantilever beam, it is necessary to consider the mechanics of the structure. Details of the theory may also assist in the design of beams with different profiles. For the problem of an out-of-plane displacement due to the internal stress of a thin film (beam), there is no conventional loading to the beam. Therefore, the Euler–Bernoulli beam equation is more useful in the form given in (2)

$$EI\frac{d^2z}{dx^2} = M(x) \tag{2}$$

where E is the elastic modulus of the beam, I is the moment of inertia, $M(x)$ is the moment acting on the beam as a function of the x-position, and z is the deflection of the beam as a function of x. This form is applicable to this beam, since there is no y-directed external load from which to calculate bending moments; however, it is possible to obtain a form for the moment acting on the beam through the following analysis.

The beams of interest in this study are constructed with two layers of gold with different internal stresses, creating a stress gradient through the thickness of the beam. The initial curvature of the beam can be established by modeling it as a bimetallic

structure, where both layers have elastic properties of gold, but different initial stress states. Consider a bimetallic structure of length L, width w, thickness b, composed of a highly stressed layer of stress σ_1 and a bottom substrate of stress σ_2. A rectangular coordinate system is set up with the x-direction along the length of the beam, the y-direction along the in-plane thickness of the beam, and the z-direction along the through-plane width of the beam.

Assuming a linear stress gradient vertically throughout the entire beam, and uniform top layer, (3) represents the stress at any point in the beam

$$\sigma(y) = \frac{\sigma_1 + \sigma_2}{2} + \frac{\sigma_1 - \sigma_2}{b} y. \tag{3}$$

The vertical distance from the centerline of the structure is y. Since the first term in this expression is constant for all beam positions, it may be dropped from our analysis. This is due to the fact that it is not the magnitude of the stresses but the difference between their values that gives rise to the deflection of the cantilever.

In the case where the upper, more highly stressed layer is not spatially uniform, the analysis changes, as shown in Fig. 2. In the fabrication of the newly developed structures, the stressed layer was patterned so as to create a linear variation in the through-plane stress (y-direction), along the length of the beam (x-direction). As mentioned in the introduction, a lithographic patterning method was used to demonstrate this desired stress gradient in the x-direction; however, many alternate approaches can be considered. The upper, stressed gold layer was deposited in the shape of a triangle (see Fig. 2). The equation for stress was modified to represent this new geometry where the stress difference linearly increases from zero at $x = 0$ and attains a maximum value at $x = L$. Equation (4) shows the representation of stress

$$\sigma(y, x) = (\sigma_1 - \sigma_2) \cdot \left(\frac{y}{b}\right) \cdot \left(\frac{x}{L}\right). \tag{4}$$

Integrating to find the total moment results in (5)

$$\begin{aligned} M(x) &= \int_{-b/2}^{b/2} dM = \int_{-b/2}^{b/2} y \cdot dF \\ &= \int_{-b/2}^{b/2} y \cdot \sigma(y, x) \cdot w \cdot dy \qquad (5) \\ &= \int_{-b/2}^{b/2} (\sigma_1 - \sigma_2) \cdot \left(\frac{y}{b}\right) \cdot \left(\frac{x}{L}\right) \cdot w \cdot y \cdot dy \\ &= (\sigma_1 - \sigma_2) \cdot \frac{b^2 w}{12 \cdot L} \cdot x. \qquad (6) \end{aligned}$$

Note, the stresses are in plane with the beam, and the moment calculated is due to integrating the value of this in-plane stress through the y-direction [2]. For the analysis of the beam with the patterned stressed layer, the moment varies linearly with the x-position of the beam, as shown in (6). It should also be noted that the thickness of the beam, b, varies linearly along the beam length as $b(x) = b_0 + (x/L)b_s$, where b_0 is the thickness of the soft gold layer and b_s the thickness of the stressed gold layer. Therefore the moment of inertia of the beam, I, also varies along the beam length, $I(x) = (1/12)w\,[b(x)]^3$. From this analysis, (2) takes the following form:

$$\frac{d^2 z}{dx^2} = \frac{(\sigma_1 - \sigma_2)}{E} \frac{x}{b_0 L + x b_s}. \tag{7}$$

Solving (7) subject to the boundary conditions of zero slope and zero deflection at the fixed end, the following expression for deflection $d(x)$ of the cantilever beam is obtained:

$$\begin{aligned} d(x) &= \frac{\sigma_1 - \sigma_2}{E b_0 L} \\ &\quad \times \left(\frac{x}{a^2} + \frac{x^2}{2a} - \frac{\ln(1 + ax)}{a^3} - \frac{x \ln(1 + ax)}{a^2} \right) \\ \text{where } a &= \frac{1}{L} \frac{b_s}{b_0}. \end{aligned} \tag{8}$$

When the above results are compared to the results of the analysis performed for a structure with a uniformly stressed hard gold layer, a relationship is developed to describe the differences in beam shape due to the different stressed layer geometry. Equation (9) shows the quantitative difference in beam shape for the patterned stress-layered (see Fig. 2) devices and the uniform stress-layered devices [3]

$$\begin{aligned} \frac{d_{\text{patterned}}(x)}{d_{\text{uniform}}(x)} &= \frac{2}{aL} \\ &\quad \times \left(\frac{1}{ax} + \frac{1}{2} - \ln(1 + ax) \left(\frac{1}{a^2 x^2} + \frac{1}{ax} \right) \right) \end{aligned} \tag{9}$$

where $d_{\text{patterned}}(x)$ is the calculated deflection of the patterned hard gold beam as a function of distance x along the length of the beam. For a ratio of hard gold thickness to soft gold thickness equal to 0.1, (9) yields an end beam deflection ratio ($x = L$) of approximately 0.32, about one-third. This same approach can be used to construct beams of different deflections by proper design of the hard gold pattern.

III. Experimental Procedure

The processing sequence used to create the cantilever beam devices examined in this study has been reported previously [3]. One additional processing step was performed in order to pattern the triangular stressed gold regions. The process sequence began with the deposition of 1.0 μm of aluminum onto a bare silicon wafer by dc sputtering. The aluminum is patterned into electrodes with the first photolithography step. BCB polymer (Cyclotene 4022, 25 wt%) was chosen for the dielectric material needed to insulate the bottom electrode. A 1.5-μm-layer of BCB was deposited onto the bottom electrodes, and the BCB was subsequently patterned. To form the anchor base, a 300-Å-layer of titanium was deposited to aid in the adhesion of 1 μm of gold. An electron-beam evaporator was used to deposit the titanium and gold layers.

Shipley 1813 photoresist was spun onto the wafer (over the anchors) to form the 2.5-μm-thick release layer. The wafer was then patterned, and the seed layer for electroplating was deposited. The seed layer consisted of 300 Å of titanium (adhesion) and 2000 Å of gold. A 2-μm-layer of soft gold was electroplated onto the seed layer at a bath temperature of 60 °C and at a current density of 3 mA/cm^2.

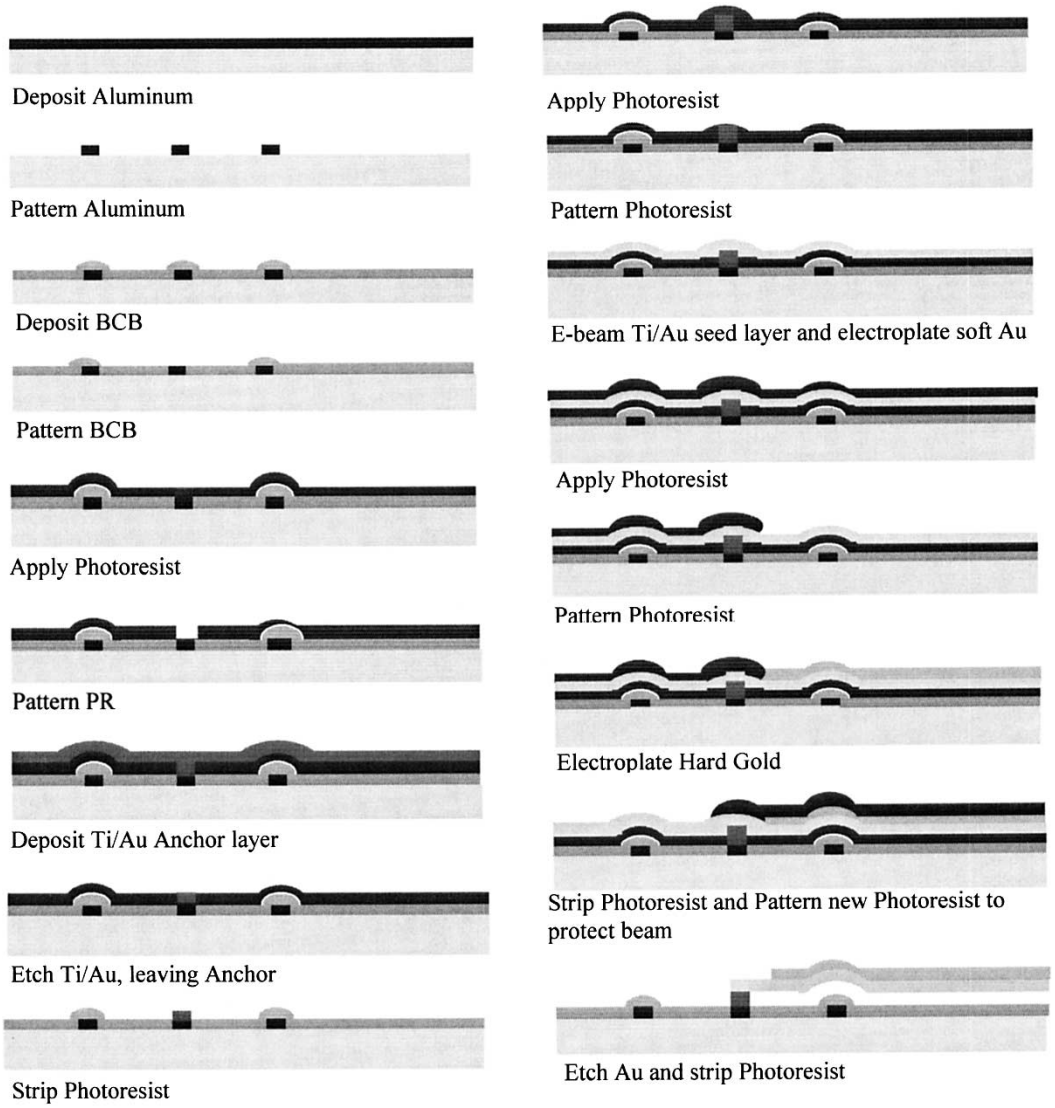

Fig. 3. Schematic of processing sequence.

The triangular-shaped hard gold pattern was formed after the soft gold electroplating. Shipley 1813 photoresist was used to protect the hinges and other parts of the device where hard gold was not desired. A 0.2-μm-layer of hard stressed gold was electroplated selectively in these opened regions at a current density of 5 $\mathrm{mA/cm^2}$ and at room temperature.

The resist selectively covering the plane of soft gold was then stripped in acetone. After using Shipley 1813 photoresist again in order to pattern the beam and hinge shapes, the unwanted gold was etched with a $\mathrm{I_2/KI}$ etchant, and the titanium was etched with an EDTA solution. Finally, the beams were released by dissolving the resist with acetone. The full process sequence can be found in Fig. 3.

After the top electrodes were released, they were treated with two low surface tension solvents, methanol and ethanol, ensuring the removal of water from the surface of the gold. The top electrodes were then exposed to an alkane thiol solution that forms a hydrophobic, self-assembled monolayer over the gold surface. This prevented stiction of the top electrodes to the bottom surface.

Fig. 4(a) shows an SEM of the fabricated device. From this image, the nonuniform curvature is clearly visible. The beam is initially flat, but the radius of curvature decreases along the length of the beam. A top-down view in an optical microscope shows the patterned hard gold shape (Fig. 4(b)).

After the devices were treated with the alkane thiol, they were measured and tested in a low-temperature microprobe station (MMR Technologies). The probe station was evacuated with a Pfeiffer Vacuum TCP 015 turbo pump and the temperature was controlled between 77 K and 400 K via a resistance heater and Joule-Thomson cooler. The position of the cantilever beam was measured and viewed with an optical microscope through a quartz window.

In addition to device testing, modeling was performed using the MEMCAD simulation package from Coventor to compare device characteristics between laboratory measurements and simulation through finite element methods. For the model of the patterned hard gold device, a single square layer was constructed with built-in variable stresses both along the beam length (x-direction) and through the depth of the structure (y-direction).

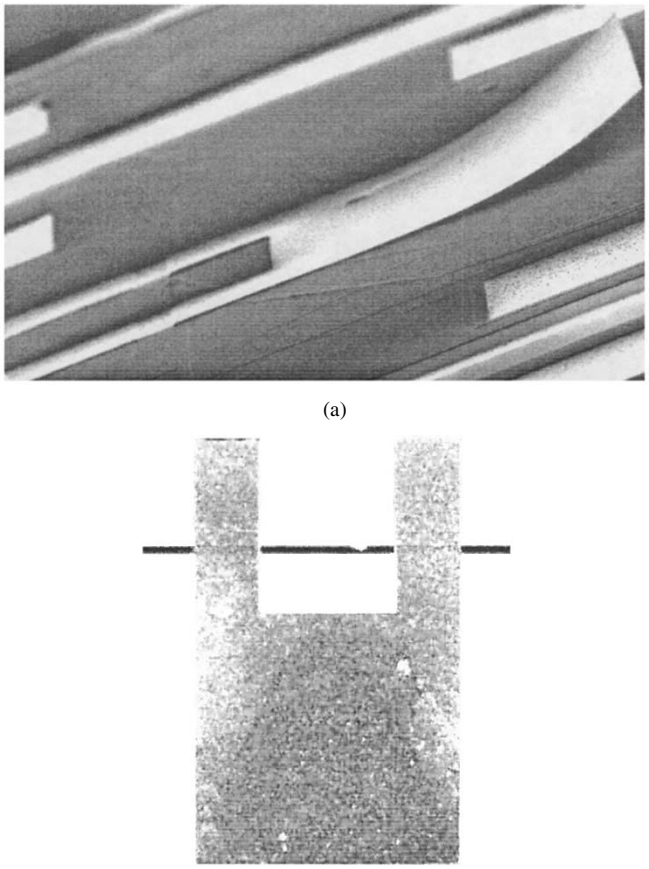

(a)

(b)

Fig. 4. SEM and optical micrograph of fabricated device.

IV. Results

The effects of shape and dimensions of the cantilever beam on its electrostatic movement were investigated. Fig. 5 shows the layout of four devices that were fabricated, tested, and measured. In this figure, the shape and size of the top electrode, shape of the bottom electrode, and shape of the stressed gold are shown. The hinge configuration, and beam length, width and tip slope were varied to investigate advantages inherent to different geometries. Note, the tuning range is defined as the percentage of the initial deflection the device tip can be moved before instability results in a snapping-down of the cantilever to the substrate.

A. Device Testing and Modeling: Double-Hinged Square

The first device to be studied was a double-hinged square as shown in Fig. 5(a). Fig. 6 shows the distance between the tip and the bottom electrode (tip deflection) versus voltage for a double-hinged, square device. The distance (height) was measured between the midpoint of the end of the beam (the tip) and the substrate. For the uniformly stressed, double-hinged, square device, the initial tip deflection was $205\pm5\ \mu\mathrm{m}$ (curve 6a). The beam became unstable between 65 and 70 V and snapped-down onto the bottom electrode.

The double-hinged square uniform hard gold device was modeled to help understand the deflection and movement with applied voltage. The model was obtained by performing an iterative sequence of simulations at regular voltage intervals between 0 V and 100 V. Fig. 7 shows the modeled voltage vs. deflection curves for both the patterned and uniform gold versions of the double-hinged square device. There is a sharp pull down at approximately 70 V, and this result agrees well with the experimental result shown in Fig. 6(a). Both the pull-down value and the shape of the deflection curve for the uniformly stressed structures are in agreement with experimental results previously documented [2], [3]. This example clearly shows the nature of the instability problem. Only a small deflection was possible under controlled conditions. Although a simple spring model predicts 1/3rd of the displacement can be carried out under controlled conditions, often (as in Fig. 6(a), the value is less. In Fig. 6(b), the initial deflection for the double-hinged, square device containing a variable stress gradient was $143\pm5\ \mu\mathrm{m}$. This deflection is about 70 percent of the deflection of the uniformly stressed square device. The average intrinsic stress for the patterned devices was less than the stress for the uniformly patterned devices; therefore the initial deflection for the variably stressed devices was smaller. Upon the new variable stress gradient, the double-hinged square device could now be tuned across 70 percent of the possible range. This is a very significant improvement over the uniform layer in Fig. 6(a). Approximately 25 of each beam type were energized and examined. The results were found to be repeatable.

Upon application of an applied voltage to the variably stressed double-hinged square device, the top electrode smoothly pulled down between 150 and 250 V. The tip contacted the bottom electrode between 280 and 290 V. The voltage pull-down of the variably stressed hard gold device was modeled. The simulation of the variably stressed gold device yielded an initial deflection of $110\ \mu\mathrm{m}$ and a more gradual pull-down compared to the uniformly stressed gold structure. One difference between the finite element MEMCAD model and the analytical solution in the Theory section is that z-direction (width) variations were not considered. Fig. 7 shows this improved pull-down behavior predicted by the modeling. The calculations showed a lower initial deflection ($110\ \mu\mathrm{m}$) than what was observed experimentally [see Fig. 6(b)]. The model predicted a gradual curve toward the point of instability. The curve in Fig. 7 shows the model for the patterned device began to deflect between 20 and 30 V (more sharply than the fabricated devices). In spite of this difference in scaling, the absence of a limited tuning range immediately followed by a sudden pull-down instability in the voltage versus deflection profile for the patterned hard gold device indicates that a different mechanism of pull-down is at work. Instead, it appears that the beam with patterned hard gold uncurls gradually onto the dielectric layer with the application of increasing voltage. Modeling gives support to this observation.

B. Modeling: Pull-Down Analysis

The gradual uncurling pull down can be further supported by modeling the area of the beam in contact with the underlying dielectric as a function of voltage. Fig. 8 (uniformly stressed gold layer) shows the percent area in contact between the cantilever beam and the lower electrode. As can be seen, the contact area

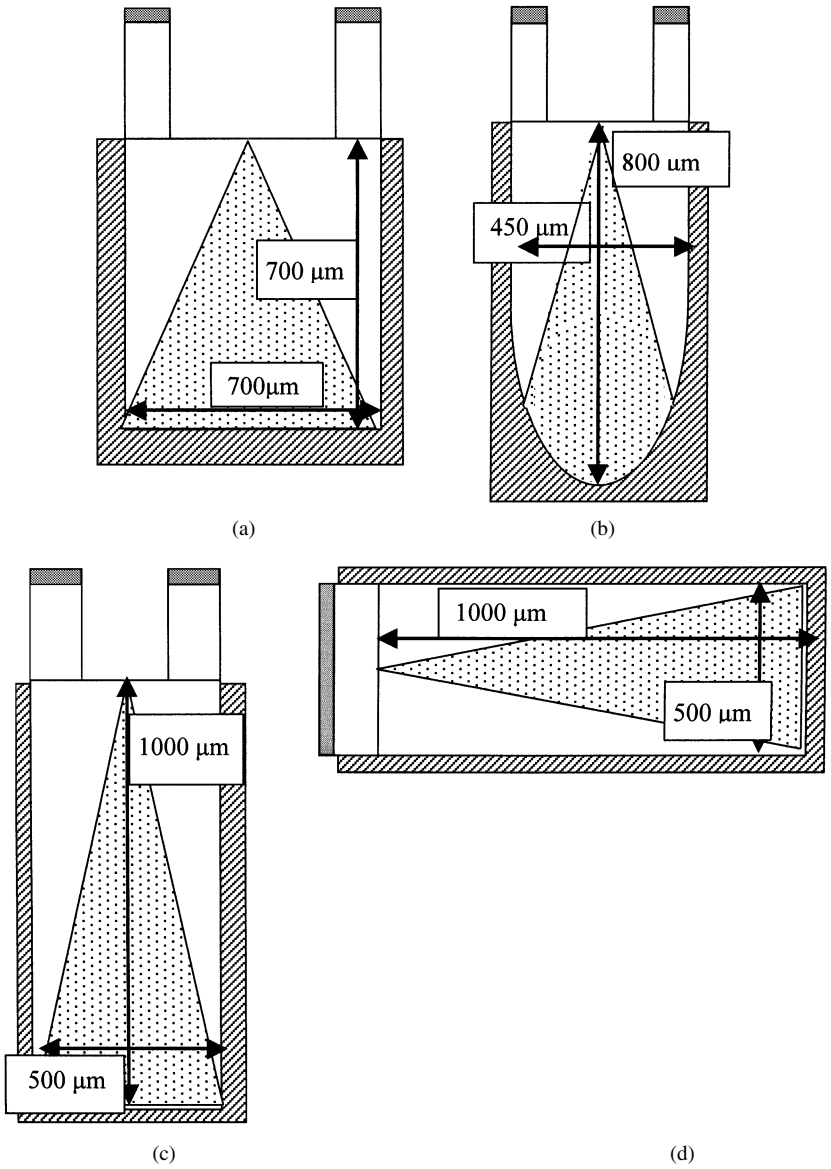

Fig. 5. Shapes and dimensions of cantilevers, bottom electrodes, and stressed gold.

increases from zero just below the pull-down voltage to approximately 75% at pull-down. Note, that the entire bottom area of the cantilever cannot easily be pulled into contact with the dielectric. Here, the area close to the hinge does not make contact, since one end is fixed above the plane of the BCB.

The model does not predict the same pull-down for the variably stressed gold device. Since the hard gold width increases along the length of the beam, the radius of curvature of the cantilever is not constant with length. Instead, the curvature radius begins at an infinite value at the hinge and decreases along the beam length to the constant value found in the case of the uniform devices. This results in the variably stressed gold device having a large portion of the cantilever positioned in closer proximity to the lower electrode. The separation is such that a much smaller voltage applied to the dc electrode will result in a movement of the actuator. However, instead of this voltage being sufficient to pull down the entire beam, it is only pulls down the part of the beam closest to the electrode. Since the beam experiences increasing curvature along its length, a further increase in voltage is necessary to further deflect the device. At each point along the pull-down the device the average radius of curvature is smaller than at lower deflections. In addition, the length of the moment arm of the device decreases as more of the beam is brought into contact with the dielectric (see Fig. 8). The combination of these two effects counteracts the instability encountered with previous devices. This theory of pull-down is consistent with the observations from device testing.

Further improvements in this beam could be made. For example, the method of inducing a linear stress gradient along the length of the beam (x-direction) could be improved by replacing the triangular hard gold layer with one where the thickness of gold varies alone the length in a known fashion. This would eliminate the unaccounted for stress gradient along beam width (z-direction). Also, the thickness and shape of the stress gold could be further investigated in order to yield a device that pulls down in accordance with a desired voltage versus deflection profile.

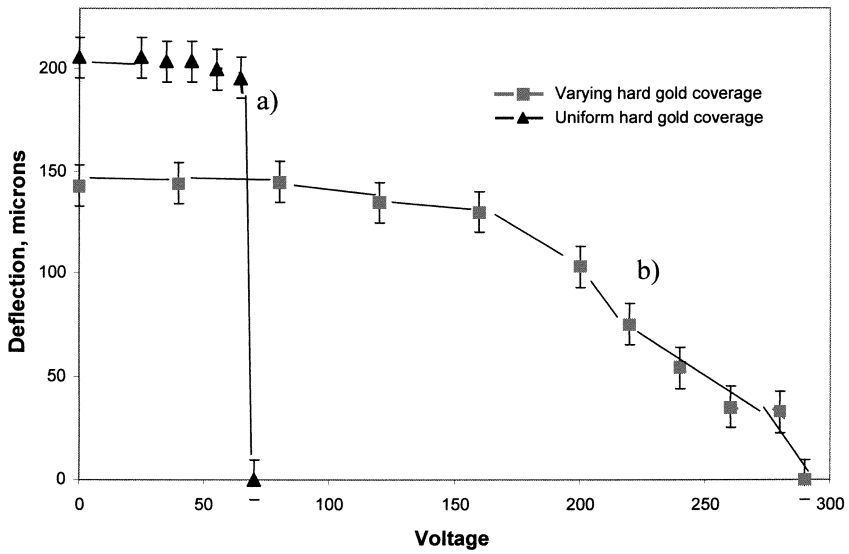

Fig. 6. Uniform vs. varying stress on a double-hinged, square device.

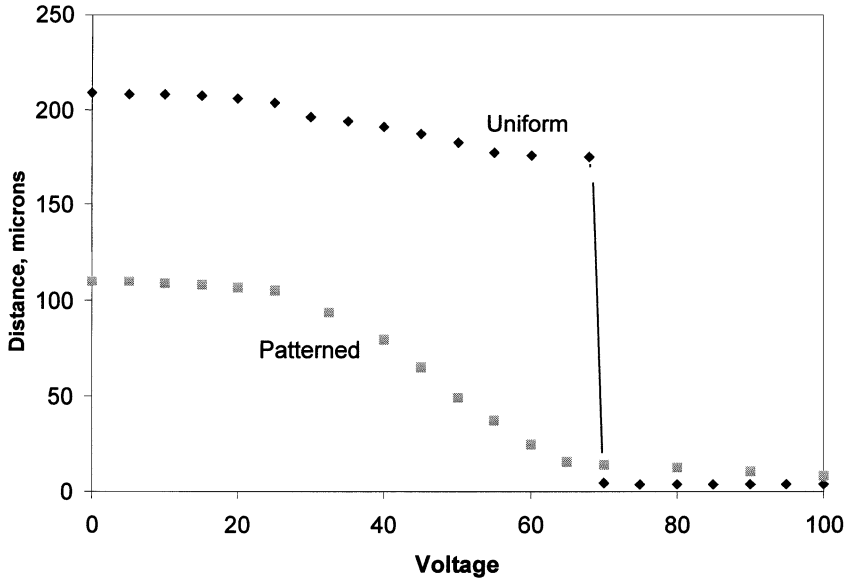

Fig. 7. Voltage cycle model for variably and uniformly stressed, double-hinged, square devices.

C. Device Testing and Measurements: Hinge and Tip Variations

A variety of beam shapes and hinge types were fabricated and measured. The distance between the tip of the cantilever and the bottom electrode (tip deflection) versus applied voltage for a double-hinged, elliptical device [see Fig. 5(b)] is shown in Fig. 9. This design was studied to mitigate the problems associated with the sharp corners on the square and rectangular devices. For the uniformly stressed double-hinged elliptical device the initial tip deflection was 250 ± 5 μm, as shown in Fig. 5(a). As the voltage increased from 0 to 70 V, the tip deflection showed little change. The distance was measured between the midpoint of the end of the beam ($x = L$ and $z = w/2$) and the substrate. The beam became unstable at 70 V and snapped-down onto the bottom electrode, as shown in Fig. 9(a). Like the double-hinged, square device, the tuning range for the elliptical device with a uniform layer of hard gold was less than one-third of the initial displacement. Upon varying the stress gradient along the length of the same shaped structure, the tuning range improved to about 45% of the initial deflection. The initial deflection for the double-hinged, elliptical device containing a varying stress gradient was 105 ± 5 μm, as shown in Fig. 9(c). Upon the application of higher applied voltages between 60 and 160 V in Fig. 9(c), the electrode smoothly pulled down. The beam tip finally rolled-down to make contact with the bottom electrode at approximately 170 V. Fig. 9(b) and (c) show the voltage deflection behavior before and after cycling of the double-hinged, elliptical device for 500 cycles, respectively. At cycle 500, the beam had a slightly higher initial deflection, resulting in a higher final pull-down voltage. This behavior was typical for the metal beams where there was an initial "break-in" period (first few cycles), followed by a very reproducible deflection versus voltage curve. This is expected because there is no chemical reaction between the layers since they are both gold. Further, the grain structure of the gold

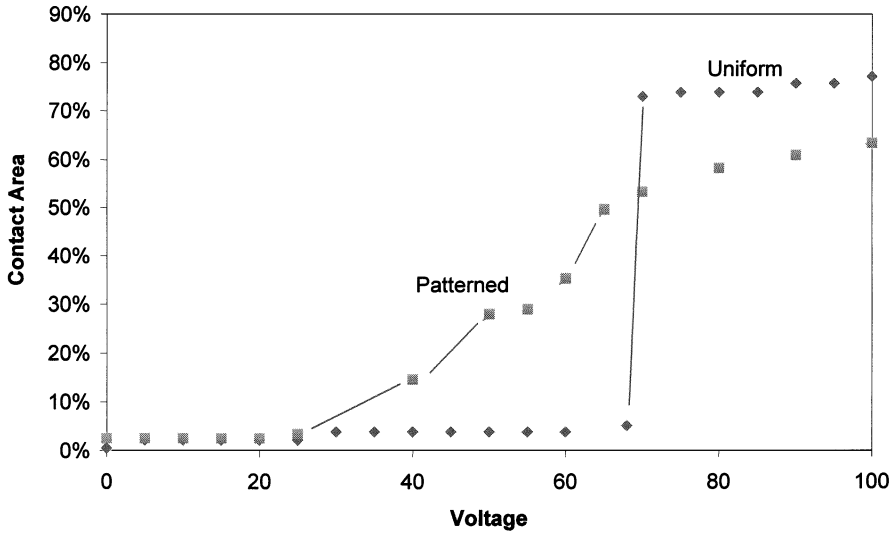

Fig. 8. Contact area versus voltage for pull down analysis of variably and uniformly stressed, double-hinged, square devices.

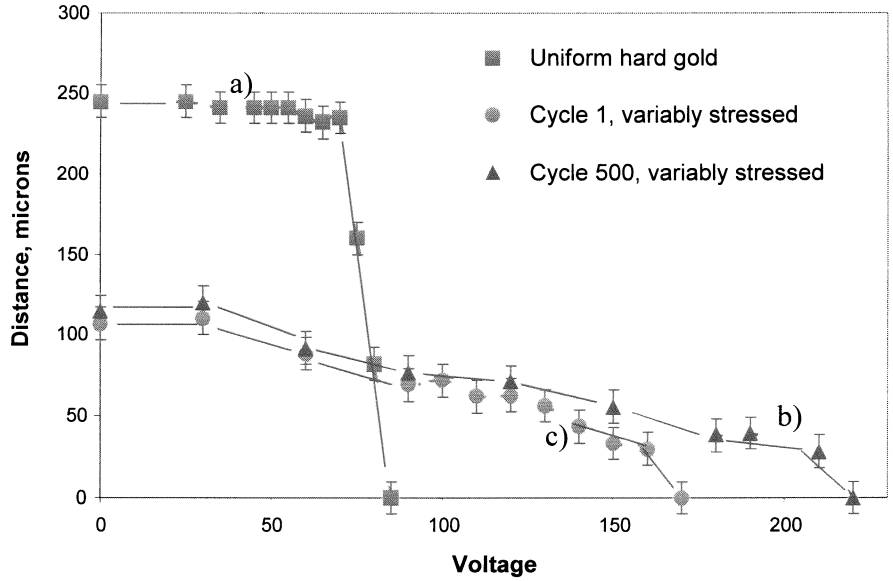

Fig. 9. Uniform versus varying stress on a double-hinged, elliptical device.

layers is known to be stable over long periods of time (30 year reliability of hard gold in electronic uses) [5].

The third double-hinged beam to be measured was the double-hinged, rectangular device [see Fig. 5(c)]. Fig. 10 shows the distance between the tip and the bottom electrode (tip deflection) versus voltage for a double-hinged, rectangular device. For the rectangular device with a uniform layer of hard gold (Fig. 10, curve a), the initial tip deflection was $230\pm5\ \mu\mathrm{m}$. As the voltage increased from 0 to 50 V, the beam moved monotonically to a deflection of $150\pm5\ \mu\mathrm{m}$ (approximately $d = 2/3$), after which it snapped down 70 V. Upon varying the stress gradient along the length of the same structure (variably stressed gold), the tuning range improved from 35% to 65% of the possible range [see Fig. 11(b)]. Other devices with the same shape and stress gradient were measured and showed the same tuning range.

The final beam measured was the full-hinged, rectangular device [see Fig. 5(d)]. Fig. 11 shows the distance between the tip and the bottom electrode (tip deflection) versus voltage for a full-hinged rectangle. For the rectangular device with a uniform layer of hard gold, the initial tip deflection was $230\pm5\ \mu\mathrm{m}$ [see Fig. 11(a)]. As the voltage increased from 0 to 60 V, the beam moved monotonically to a deflection of $200\pm5\ \mu\mathrm{m}$. The beam became unstable between 60 and 80 V. Upon varying the stress gradient along the length of the full-hinged, rectangular device, the initial tip deflection decreased by about 35 percent to $150\pm5\ \mu\mathrm{m}$ [see Fig. 11(b)]. The tip deflection changed slightly with voltage up to 140 V for the variably stressed, full-hinged, rectangle. The beam became unstable between 140 and 160 V. The full-hinged, rectangular device with a two-axis stress gradient shows a different deflection behavior than the partial-hinged cantilevers. The difference in behavior can be attributed to the effect of the anchor. The full-hinged, rectangular device has higher rigidity than the double-hinged structures since deflection of the double-hinged structures required bending about an arm of less width.

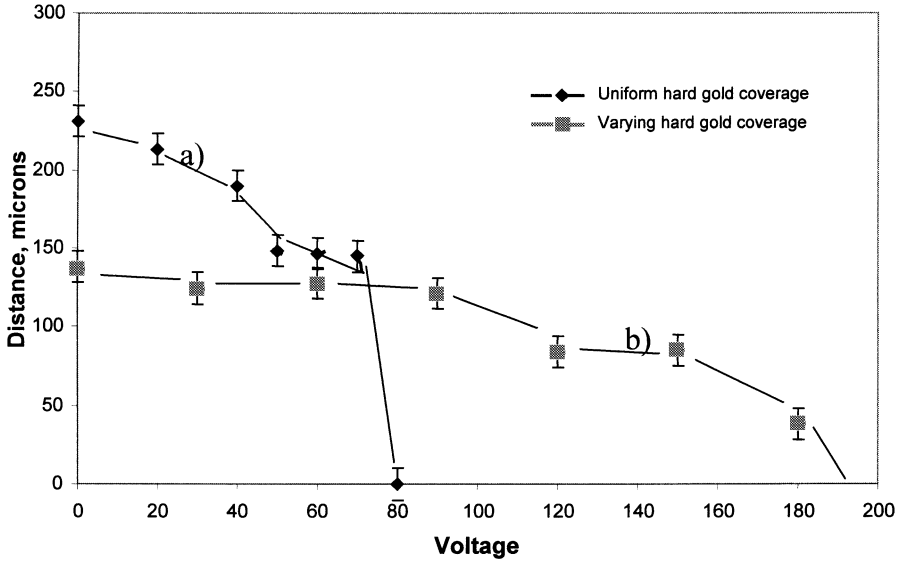

Fig. 10. Uniform vs. varying stress on a double-hinged, rectangular device.

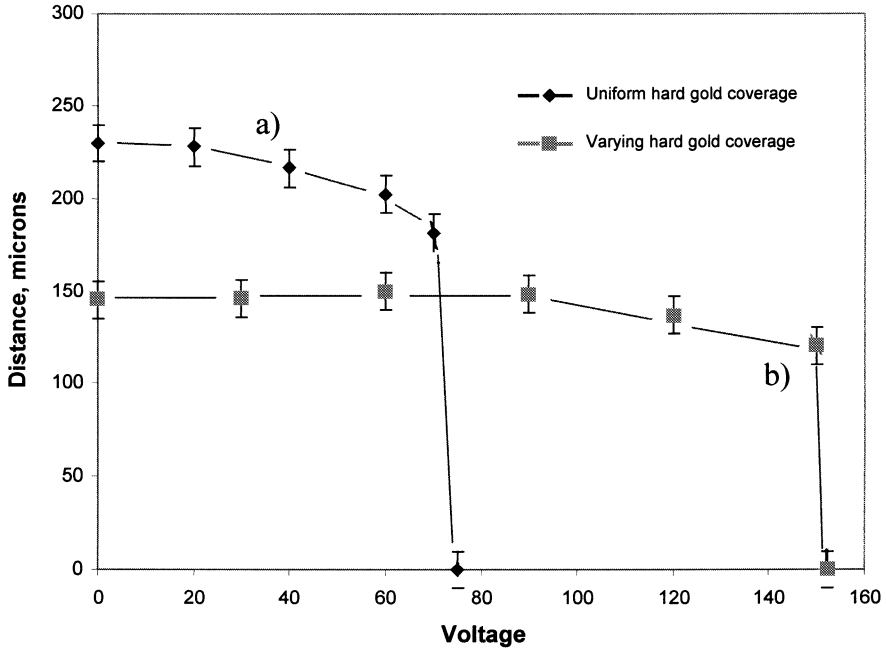

Fig. 11. Uniform vs. varying stress on a full-hinged, rectangular device.

Initial deflection, pull-down voltage, and deflection at pull-down were measured and compared to other devices, as well as between corresponding patterned and uniform hard gold structures. Both the initial deflection and pull-down voltage were found to be systematically different between uniform and patterned hard gold structures of comparable geometry. The results are summarized in Table I. Pull-down voltage, tuning range, and initial deflection are given for the patterned and uniform stressed-gold versions of each of the four devices discussed. All data is after devices have been through 500 cycles. The patterned hard gold devices had increased tuning range at the cost of higher pull-down voltage for each of the double-hinged devices. The fully hinged rectangular structure saw no improvement with the addition of the stressed gold.

D. Modeling: Beam and Tip Geometry

Analysis of these devices shows the advantages of the elliptical structures versus rectangular structure. The elliptical geometry showed a ratio of two-fifths for the initial deflection of the patterned device to the uniform device, and the rectangular geometry has a value of close to two-thirds for this ratio (both in excess of the one-third value). This serves as evidence that the nature of the beam tip may be significantly enhanced at low deflections by curvature along the width of the beam. That is, the

TABLE I
SUMMARY OF DEVICE VOLTAGE VERSUS DEFLECTION DATA

	Stressed Gold Coverage	Pull-Down Voltage, V	Initial Deflection, μm	Tuning Range, %
Double-Hinged Square	Patterned-Triangle	280	143	70
	Uniform	70	205	10
Double-Hinged Ellipse	Patterned-Triangle	170	105	45
	Uniform	80	250	10
Double-Hinged Rectangle	Patterned-Triangle	185	135	65
	Uniform	80	230	35
Full-Hinged Rectangle	Patterned-Triangle	160	150	15
	Uniform	80	230	20

presence of the hard gold appears to contribute substantially to the deflection of rectangular devices by elevating the beam tip at the corners. Thus, the width of the device plays an important role in determining the overall cantilever shape and control.

The deflections reported for the modeling correspond to the largest deflection at any point along the beam. With the exception of the double-hinged, square device, the actual devices did not exhibit a large observable variation in deflection along the width of the tip. Modeling predicted the difference was greatest for wide devices with relatively low end-beam slope. In simulations of the double-hinged square device, modeling found the out-of-plane curvature along the beam width accounted for up to a 40-μm variation in deflection from the center of the tip to either corner. Subtracting the difference in deflection from the beam corner to the center of the beam tip, the ratio of the center-tip deflection of the variably stressed device to the uniformly stressed device was found to be approximately two-fifths.

E. Capacitance Modeling

The results have been focused on improvements in beam design. To simulate the action of a variable capacitor, a small aluminum electrode was placed under the beam tip, electrically independent of the dc electrode. This represents the plate of the variable capacitor in the working device. By applying a voltage to the dc electrode to change the beam position, the change in capacitance between the beam and the second electrode was evaluated. Fig. 12 shows the modeling results for the capacitor. There is a significant benefit of the patterned hard gold device in terms of the capacitance-voltage response. The uniformly stressed gold structure experiences an increase of capacitance on the order of 10% before snapping down (Fig. 12, uniform stressed gold), the patterned hard gold device exhibits a continuous capacitance increase close to 100% of its value before the slight snap-down to the lower layer near 60 V (Fig. 12, variably stressed gold). This is an order of magnitude improvement in the potential tuning range of the variable capacitor devices.

F. Temperature Effects

The effects of temperature on two of the devices discussed above were investigated. Temperature cycling experiments were performed on the double-hinged square and the double-hinged, elliptical devices. Both devices were fabricated with the variably stressed gold layer. A decrease in elastic modulus at lower temperatures has been previously reported [6]. At room temperature, the elastic modulus for bulk gold is 78 ± 1.5 GPa. At 200 K, close to the low temperature used here, the elastic modulus increased to 81 ± 1.5 GPa. Equation (10), Stoney's Equation, relates the intrinsic stress of the beam to the elastic modulus and geometry of the beam

$$\sigma = \frac{E_{\text{sub}}}{6(1-\nu_{\text{sub}})}\frac{h_{\text{sub}}^2}{t_{\text{film}}R} \tag{10}$$

where E is the elastic modulus of the substrate, ν is Poisson's ratio for the substrate material, σ is the intrinsic stress of the hard gold, t is the hard gold thickness, h is the soft gold substrate thickness, and R is the radius of curvature of the beam. Temperature also affects the thermal expansion coefficient. As temperature increases, the length of the beam expands, which causes the stress in the beam to change. Fig. 13 shows the temperature effects on a double-hinged, square device with a variably stressed layer. The curve at room temperature is the same curve shown in Fig. 6, displaying an initial deflection of 143 ± 5 μm. When the temperature is lowered from room temperature to 225 K, the voltage versus displacement curve shifts slightly above the curve obtained at room temperature. In Fig. 13, the initial tip deflection increased to 155 ± 5 μm, higher than the value at room temperature. At low temperature, the beam follows the same path as the room temperature curve, and snaps-down at the same voltage. The voltage vs. deflection curve for the structure at 395 K shows that the device comes into contact with the bottom electrode at approximately 220 V. This behavior (see Fig. 13) is in sharp contrast to bimetallic beams whose coefficient of thermal expansion difference results in very significant changes with temperature.

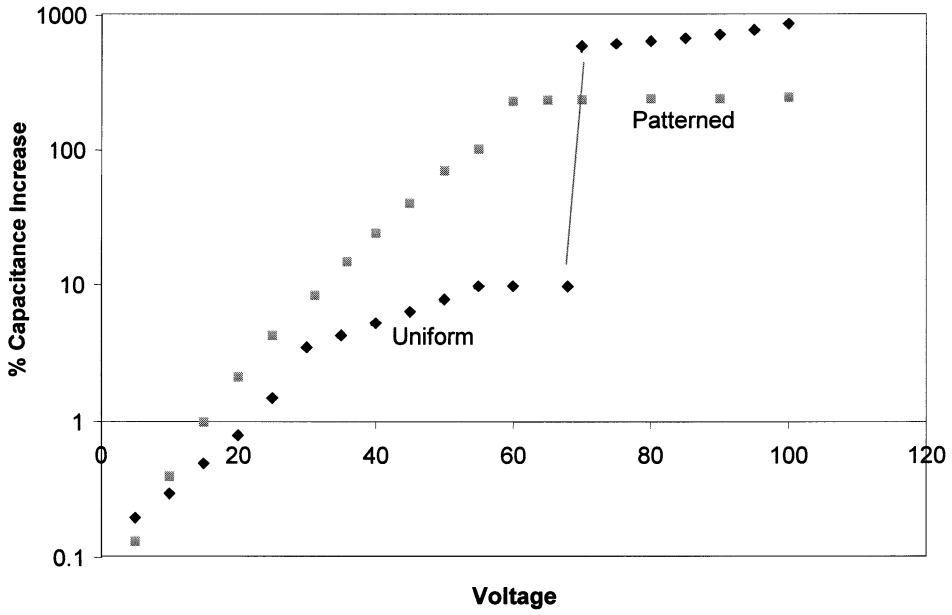

Fig. 12. Capacitance model for variably and uniformly stressed, double-hinged, square devices.

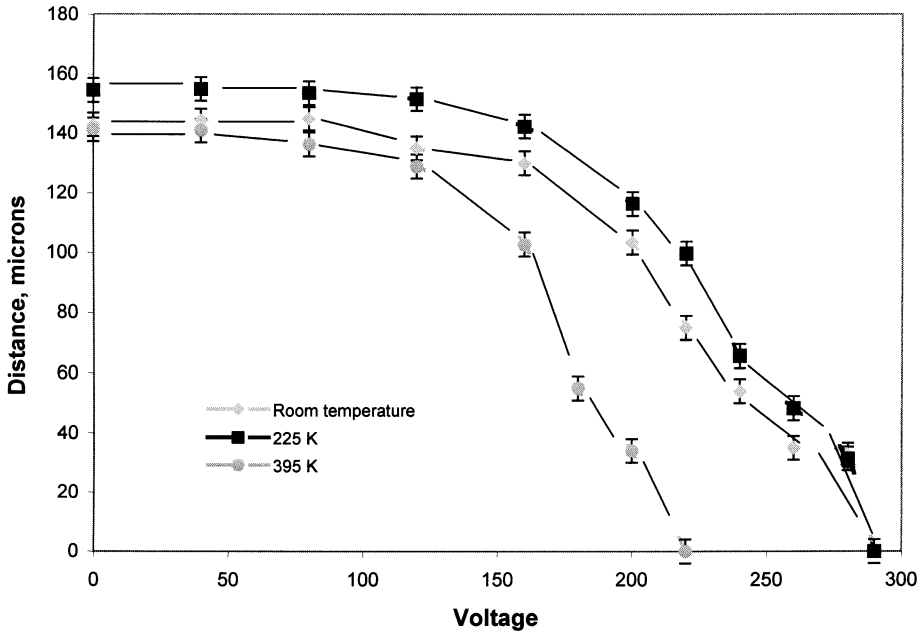

Fig. 13. Temperature cycling for a double-hinged, square device.

V. Conclusion

The pull-down characteristics of four electrostatic actuators were measured. Stressed, hard gold was patterned in a triangular shape on top of stress-free soft gold. This induced a variable stress gradient in the cantilever beams that varied with beam thickness and length. This stress gradient along the length of the beams significantly improved the tuning range compared with devices containing spatially uniform stress. The tuning range of the variably stressed gold devices improved to 70% for the double-hinged square devices, to 45% for the double-hinged elliptical devices, and to 65% for the double-hinged rectangular device. The anchor arrangement affects the pull-down behavior of the top electrode, as shown by the full-hinged, rectangular device. The double-hinged arrangement provides more freedom of motion. Voltage cycling had an initial impact on the pull-down characteristics of the actuator, but no observed drift after 500 cycles. Modeling predicts a gradual pull-down curve for the variably stressed devices, which was confirmed by experimental results.

Acknowledgment

Significant contributions by E. Prophet, B. A. Willemsen, and J. Musolf of Superconductor Technologies, Inc., in the

form of technical insight and valuable discussion are greatly appreciated.

REFERENCES

[1] J. J. Yao, "RF MEMS from a device perspective," *J. Micromech. Microeng.*, vol. 10, pp. R9–R38, 2000.

[2] A. K. Chinthakindi, D. Bhusari, B. P. Dusch, J. Musolf, B. A. Willemsen, E. Prophet, M. Roberson, and P. A. Kohl, "Electrostatic actuators with intrinsic stress gradient. Part-I. materials and structures," *J. Electrochem. Soc.*, vol. 149, pp. H139–H145, 2002.

[3] A. K. Chinthakindi and P. A. Kohl, "Electrostatic actuators with intrinsic stress gradient. Part-II," *J. Electrochem. Soc.*, vol. 149, pp. H146–H152, 2002.

[4] E. S. Hung and S. D. Senturia, "Extending the travel range of analog-tuned electrostatic actuators," *Journal of Microelectromechanical Systems*, vol. 8, pp. 497–505, December 1999.

[5] P. A. Kohl, "Electrodeposition of gold," in *Modern Electroplating*, M. Schlesinger and M. Paniov, Eds. New York: Wiley, 2002.

[6] H. Tanimoto, S. Sakai, Y. Koda, K. Otsuka, E. Kita, and H. Mizubayashi, *Mechanical Properties of Nanocrystalline Gold After Low-Temperature Irradiation. 4.5*.

Gary D. Gray received the B.S. degree in chemical engineering from Georgia Institute of Technology, Atlanta, in 2000. He is currently working toward the M.S. degree in physics and the Ph.D. degree in chemical engineering at the same.

Matthew J. Morgan received the degree in chemical engineering at the Georgia Institute of Technology, Atlanta, and the M.S. degree in chemical engineering in 2002.

Paul A. Kohl (A'92–M'02) received the Ph.D. degree in chemistry from The University of Texas at Austin in 1978.

He is Regents' Professor of chemical engineering at the Georgia Institute of Technology, Atlanta. He was employed at AT&T Bell Laboratories from 1978 to 1989. At Bell Laboratories, he was involved in new materials and processing methods for semiconductor devices. In 1989, he joined the faculty of the Georgia Institute of Technology, where he is currently a Regents' Professor. His research interests include ultra low-k dielectric materials, interconnects for microelectronic devices, and electrochemical energy conversion devices. He has over 120 journal publications, and 30 patents.